

Investigating clustering dark energy with 3d weak cosmic shear

Youness Ayaita¹, Björn Malte Schäfer², and Maik Weber^{★1}

¹ *Institut für Theoretische Physik, Universität Heidelberg, Philosophenweg 16, 69120 Heidelberg, Germany*

² *Astronomisches Recheninstitut, Zentrum für Astronomie, Universität Heidelberg, Mönchhofstraße 12, 69120 Heidelberg, Germany*

18 October 2018

ABSTRACT

As observational evidence increasingly consolidates the case for a cosmological constant Λ being the source of the Universe’s accelerated expansion, the question whether, and if so, how well, future experiments could detect deviations from this standard scenario is raised with urgency. Assuming a dark energy component different from a cosmological constant, the observable effects in general include gravitational clustering described by the fluid’s (rest–frame) speed of sound c_s . We employ 3d weak cosmic shear, a proposed method to take advantage of the full three–dimensional information inherent to the cosmic shear field, to explore the capability of future surveys to detect dark energy clustering and the signature of an enhanced amplitude of the matter power spectrum on large scales. For this purpose, we present adequate numerical methods facilitating 3d weak cosmic shear calculations. We find that the possible constraints heavily depend on the dark energy equation of state w . If w is not very close to -1 , constraining the squared sound speed c_s^2 within an order of magnitude seems possible with a combination of Euclid and Planck data.

Key words: cosmology: large–scale structure, gravitational lensing, methods: analytical

1 INTRODUCTION

Explaining the accelerated expansion of the Universe is one of the key tasks of cosmology today. If Einstein’s general relativity remains unaltered on cosmological scales, the observed accelerated expansion—if no local effect—is due to a cosmological constant or an unknown cosmological fluid with negative pressure, the dark energy. To this day, all major observations are consistent with a cosmological constant (Komatsu et al. 2011; Bartelmann 2010a). Its unexpectedly tiny value—the cosmological constant problem—and the fact that its energy density is comparable to that of matter just today—the coincidence problem—(see, e. g., Carroll 2001) motivate the search for alternative models of dynamically evolving dark energy.

Due to the lack of observational evidence for inhomogeneities in the dark energy, most studies have only investigated the consequences of a perfectly homogeneous dark energy component. Such a fluid is completely determined by its energy density and its equation of state w . Its direct effect is restricted to the expansion history, which indirectly causes a scale–independent modification of the growth rate of matter perturbations. In general, however, a cosmological fluid can also leave signatures, possibly scale–dependent, by virtue of its perturbations. This could be, in principle, a means to discriminate between different dark energy models.

Once we include linear perturbations, another characteristic quantity enters the scene, the sound speed c_s . This quantity defines a sound horizon such that scales outside and inside this hori-

zon can undergo different evolutions. In general, both w and c_s are necessary to describe the observable effects of a fluid. In order to explore the nature of the dark energy, cosmology has to constrain both w and c_s (Hu 2002b; Erickson et al. 2002; DeDeo et al. 2003; Hu & Scranton 2004).

The remarkable progress of observational cosmology in determining the fundamental parameters describing our Universe has not yet led to significant constraints on the dark energy sound speed c_s (Bean & Dore 2004; de Putter et al. 2010; Li & Xia 2010). In this work, we study whether next generation precision observations of the cosmic microwave background together with the proposed method 3d weak cosmic shear (Heavens 2003) have the potential of providing significant progress in this respect.

3d weak cosmic shear is a method to gain precision information about the growth of perturbations (Heavens 2003; Castro et al. 2005; Kitching et al. 2011). Contrary to ordinary galaxy surveys, it has—like weak lensing in general—the advantage of being independent of galaxy bias models. Only well–understood general relativity is needed from the theoretical side. This is one reason why weak gravitational lensing, since its beginnings (Van Waerbeke et al. 2000), has advanced along with the CMB to one of the cosmological probes with the largest potential (Huterer 2010; Bartelmann 2010b). Weak lensing methods have in fact proved to be powerful tools to constrain dark energy, i. e. mainly its equation of state parameter w (Huterer 2002; Jain & Taylor 2003; Heavens 2003; Bernstein & Jain 2004; Takada & Jain 2004; Hannestad et al. 2006; Heavens et al. 2006; Amendola et al. 2008; Hollenstein et al. 2009; Kilbinger et al. 2009; Huterer 2010).

Most weak lensing studies consider the case of tomographic

★ e–mail: M.Weber@thphys.uni-heidelberg.de

measurements where the sample of lensed galaxies is split up into redshift bins on which the standard weak lensing methods are applied (Hu 1999, 2002a). The advantage of tomography is an enhanced sensitivity due to reduced averaging along a line of sight compared to unbinned cosmic shear spectra, but the shape of the dark matter power spectrum is not measured independently from growth factors and geometry (recent studies about tomography and the relation to 3d weak lensing include Kitching et al. 2011; Schäfer & Heisenberg 2011).

The 3d version of weak lensing is a complement to standard 2d weak lensing with the aim of retaining the full three-dimensional information contained in the cosmological shear field. The starting point is to not only make use of the angular positions of lensed galaxies on the sky, but to also include their redshifts as a distance measure such that each individual galaxy provides a measure of the tidal shear.

Let us briefly explain our motivation to look specifically into 3d weak lensing as opposed to tomographic methods. Weak lensing spectra provide an integral measure of the dark matter power spectrum, weighted with the lensing efficiency function. The enhancement of the matter power spectrum due to the clustering of dark energy is restricted to large scales and would thus influence a weak lensing convergence spectrum only little. A 3d method, however, provides a direct measurement of the amplitude of the dark matter spectrum and would be better suited to distinguish enhanced spectra from unenhanced spectra and therefore to provide constraints on the properties of dark energy and its clustering. This would effectively break the degeneracy between the power spectrum shape and the lensing efficiency, consisting of the growth function and geometrical factors, such that the signature of dark energy induced clustering should be easier to observe.

The organisation of this paper is as follows. We first describe clustering dark energy in general, make contact with prominent dark energy models, and introduce a parameterisation in Sec. 2. We then explain the 3d weak cosmic shear method in Sec. 3. A brief description of the Fisher matrix method for forecasting parameter constraints is given in Sec. 4. We present adequate and efficient numerical tools in Sec. 5. Our results are shown in Sec. 6, and we conclude in Sec. 7.

2 CLUSTERING DARK ENERGY

2.1 The sound speed

The dynamics of the background and the evolution of scalar linear perturbations of a cosmological fluid are fully determined by its equation of state $w = \bar{p}/\bar{\rho}$ and its (squared) sound speed $c_s^2 = \delta p/\delta \rho$. If we describe dark energy as a cosmological fluid, coupled to other fluids only by virtue of the gravitational interaction, the natural parameters are w and c_s^2 .

The sound speed c_s^2 defines a characteristic scale $\lambda \propto |c_s|$, below which the fluid resists gravitational collapse. In turn, this means that the effects of gravitational clustering are only observable if the scale λ lies within the Hubble horizon, $\lambda \lesssim \mathcal{H}^{-1}$, where $\mathcal{H} = a'/a$ is the conformal Hubble parameter and a prime denotes a derivative with respect to conformal time τ .

In general, the speed of sound is defined by the quotient of the pressure and density perturbations, $c_s^2 \equiv \delta p/\delta \rho$. Both, δp and $\delta \rho$, however, are gauge-dependent quantities, whence we shall only consider the gauge-invariant rest-frame speed of sound defined in a frame where the velocity perturbation of the fluid vanishes, $v = 0$.

We can illustrate the role of the sound speed with the help of the evolution equations of linear perturbations, which are obtained from the general energy–momentum conservation equations $T^{\mu\nu}{}_{;\nu} = 0$. These equations are valid if there is no coupling, i. e. no energy–momentum exchange, between the fluid and other components such as matter. As usual, we split into background quantities and linear perturbations, $T^{\mu\nu} = \bar{T}^{\mu\nu} + \delta T^{\mu\nu}$, and we define $T^0_0 = -\bar{\rho}(1 + \delta)$, $T^0_i = (\bar{\rho} + \bar{p})v_i$, $T^i_j = (\bar{p} + \delta p)\delta^i_j + \Sigma^i_j$. We further define a gauge-invariant density perturbation $\Delta = \delta + 3(1 + w)\frac{\mathcal{H}}{k}(v - B)$ in Fourier space, where B is a metric perturbation defined as in Kodama & Sasaki (1984). Choosing the fluid’s rest frame $v = 0$ and a gauge where $B = 0$, we simply get $\Delta = \delta$. Describing the evolution of perturbations, for a single fluid, in terms of the variable $\rho a^3 \delta$, we find the following second-order differential equation (cf., e. g., Kodama & Sasaki 1984),

$$(\rho a^3 \delta)'' + \left(1 + 3\frac{\dot{\bar{p}}}{\bar{p}}\right) \mathcal{H}(\rho a^3 \delta)' + \left(k^2 c_s^2 - \frac{3}{2}(1 + w)\mathcal{H}^2\right) (\rho a^3 \delta) = 0, \quad (1)$$

neglecting anisotropic shear, $\Sigma^i_j = 0$. A critical scale $k_{\text{crit}} \equiv 1/\lambda_{\text{crit}}$ is given by the vanishing of the source term $\propto \rho a^3 \delta$ driving gravitational collapse, i. e.,

$$\lambda_{\text{crit}} = \sqrt{\frac{2}{3}} \frac{1}{\sqrt{1+w}} \frac{|c_s|}{\mathcal{H}}. \quad (2)$$

The perturbation variable $\rho a^3 \delta$ can only grow on subhorizon scales for $\lambda_{\text{crit}} \lesssim \mathcal{H}^{-1}$, which translates into the approximate relation $c_s^2 \lesssim 1 + w$. Especially for an equation of state w close to -1 , as preferred by current observations (Komatsu et al. 2011), this only occurs for very small sound speeds $c_s^2 \ll 1$. These effects are restricted to large scales $\lambda \gtrsim \lambda_{\text{crit}}$.

In a complete description of the perturbation evolution, we have to cope with the multi-component fluid of (at least) matter and dark energy. Nonetheless, we can still motivate a corresponding heuristic definition of an effective scale characterising dark energy clustering, see Sec. 2.3. We will then also show quantitatively how a clustering dark energy component (with constant w and c_s^2) affects the large-scale matter power spectrum $P(k)$.

The (rest-frame) sound speed c_s^2 considered here may not be confused with the adiabatic sound speed c_a^2 , which is only equal to the quotient $\delta p/\delta \rho$ for adiabatic perturbations, i. e. when the entropy perturbation is zero. In general, it is given by $c_a^2 = \dot{\bar{p}}/\dot{\bar{\rho}}$. The difference between the two quantities defines a gauge-invariant entropy perturbation $(c_s^2 - c_a^2)\delta/w$. For a fluid with constant equation of state w , the adiabatic sound speed simply reduces to $c_a^2 = w$. For a brief introduction to dark energy clustering, see Gordon & Hu (2004).

2.2 Relation to common dark energy models

2.2.1 Quintessence

The most prominent example of dynamical dark energy is standard quintessence (Wetterich 1988; Ratra & Peebles 1988), i. e. a cosmological scalar field φ with standard kinetic term and a potential $V(\varphi)$, defining a Lagrangian density $\mathcal{L} = -\frac{1}{2}\partial_\mu\varphi\partial^\mu\varphi - V(\varphi)$. For suitable choices of the potential $V(\varphi)$, the dynamics of the background field $\bar{\varphi}$ shows appealing tracker behaviours providing robustness against initial conditions.

The perturbation $\delta\varphi$ of the quintessence field usually is of little importance on subhorizon scales, the reason being that the quintessence sound speed c_s^2 is unity.

This is easily seen by explicitly writing energy density and pressure perturbations of the scalar field,

$$\delta\rho_\varphi = \dot{\varphi}\delta\dot{\varphi} + V_{,\varphi}\delta\varphi, \quad (3)$$

$$\delta p_\varphi = \dot{\varphi}\delta\dot{\varphi} - V_{,\varphi}\delta\varphi. \quad (4)$$

Since the velocity perturbation v is proportional to the field perturbation $\delta\varphi$, the rest-frame speed of sound (for $v = \delta\varphi = 0$) is $c_s^2 = \delta p_\varphi / \delta\rho_\varphi = 1$.

We conclude that the detection of a dark energy sound speed $c_s^2 < 1$ would not only challenge the Λ CDM model but standard quintessence models as well.

A class of models with very different behaviour, however, is given by coupled quintessence models (Wetterich 1995; Amendola 2000; Amendola et al. 2008). In these models, there is an energy-momentum exchange between the dark energy and other components such as dark matter or neutrinos. Dark energy can then no longer be described as an independent fluid, and the equations of Sec. 2.1 do not apply. In fact, subhorizon perturbations of the quintessence field can grow in these models. Although not considered in this work, the case of energy-momentum exchange between dark energy and matter has been parametrised and studied in the light of weak lensing (Schäfer et al. 2008; La Vacca & Colombo 2008; Caldera-Cabral et al. 2009; De Bernardis et al. 2011).

2.2.2 k -essence

Looking at Eqs. (3) and (4), the reason for $c_s^2 = 1$ in standard quintessence is the identical dependence of $\delta\rho_\varphi$ and δp_φ on $\delta\dot{\varphi}$. Formally, this could easily be changed by allowing the potential to also depend on $\dot{\varphi}$, $V = V(\varphi, \dot{\varphi})$. If this dependence can be split into two summands, we could reinterpret the $\dot{\varphi}$ dependence as a modification not of the potential but of the kinetic term.

Non-standard kinetic terms are the starting point for k -essence models of dynamical dark energy (Armendariz-Picon et al. 2000, 2001). In these models, the Lagrangian \mathcal{L} is a generic function of the standard kinetic term $X = -\frac{1}{2}\partial_\mu\varphi\partial^\mu\varphi$. It is thus possible for the sound speed c_s^2 to take any value, without violating causality (Babichev et al. 2008).

The energy density and the pressure are given by the corresponding components of the energy-momentum tensor. They read $\rho = 2\mathcal{L}_{,X}X - \mathcal{L}$ and $p = \mathcal{L}$. The equation of state $w = \bar{p}/\bar{\rho}$ and the rest-frame sound speed $c_s^2 = \delta p/\delta\rho$ (Erickson et al. 2002) are then

$$w = \frac{\mathcal{L}}{2\mathcal{L}_{,X}X - \mathcal{L}}, \quad (5)$$

$$c_s^2 = \frac{\mathcal{L}_{,X}}{\mathcal{L}_{,X} + 2\mathcal{L}_{,XX}X}. \quad (6)$$

Of course, both w and c_s^2 evolve in time and may take very different values at different epochs. The question whether the time evolution of c_s^2 could leave characteristic observational imprints was studied by Ansari & Unnikrishnan (2011). In the framework of a specific k -essence type model, 3d cosmic shear has been used to forecast possible constraints on the model parameters (Camera et al. 2010).

2.3 Parametrised clustering dark energy

A frequently employed parameterisation of dark energy, which we shall adopt here, is the w CDM model, sometimes called X CDM (Turner & White 1997). Contrary to a cosmological constant Λ with equation of state $w_\Lambda = -1$, the model allows for an arbitrary dark energy equation of state w which is taken to be constant in

time. The model is often extended to a linear evolution of w with respect to the scale factor a (for an attempt to study w as a free function, cf. Huterer & Turner 2001). The simplest generalisation for including possible clustering of dark energy is to further introduce a rest-frame sound speed c_s^2 , also constant in time. In this paper, we completely parametrise the dark energy component by constant numbers w and c_s^2 .

Dynamical dark energy such as quintessence and k -essence provides a large class of models that cannot be approximated by a simple parameterisation such as the w CDM model. In fact, the w CDM model (for constant w) does not resemble very closely *any* of the prominent dynamical models. Whenever new observational data are published, it is thus not sufficient to study constraints in the w CDM model alone, but to also study the individual dark energy models.

Nonetheless, the w CDM model is, in terms of its parameters, a somewhat minimal extension of the standard Λ CDM model, including the latter as a special case. Hence, it is a useful tool to forecast how strong the deviations from Λ CDM must be for future observations to detect them.

We now turn to the description of linear perturbations in the presence of a clustering dark energy component parametrised as above. The linear growth of perturbations is described by a growth function $g(k, a)$ that links the Newtonian gravitational potential $\Phi_k(a)$ at scale factor a to the one today Φ_k^0 according to $\Phi_k(a) = g(k, a)\Phi_k^0/a$. We shall now introduce the parameterisation for $g(k, a)$ that we use for the study of dark energy perturbations in the w CDM model.

Dark energy perturbations contribute to the gravitational potential just as matter perturbations via the Poisson equation,

$$k^2\Phi = -4\pi G a^2 (\rho_m\Delta^{(m)} + \rho_{DE}\Delta^{(DE)}) \equiv -4\pi G a^2 Q\rho_m\Delta^{(m)}, \quad (7)$$

where we have used the gauge-invariant density perturbations $\Delta^{(m)}$ and $\Delta^{(DE)}$ and introduced the quantity $Q = Q(k, a)$. It is defined via

$$Q = 1 + \frac{\rho_{DE}\Delta^{(DE)}}{\rho_m\Delta^{(m)}}. \quad (8)$$

An important effect of dark energy perturbations is their influence on the growth of matter perturbations expressed in terms of a modified growth index γ defined by $d\ln\Delta^{(m)}/d\ln a = \Omega_m^\gamma$ (Linder & Cahn 2007). As a function of Q , we may approximate (cf. Sapone & Kunz 2009; Sapone et al. 2010; Linder & Cahn 2007)

$$\gamma \approx \frac{3(1-w-A)}{5-6w}, \quad A \equiv \frac{Q-1}{1-\Omega_m}. \quad (9)$$

We follow Sapone et al. (2010), parametrising $Q(k, a)$ for the w CDM model with sound speed c_s^2 as

$$Q \approx 1 + \frac{1-\Omega_m^0(1+w)a^{-3w}}{\Omega_m^0(1-3w+y^2)}, \quad y^2 \equiv \frac{2}{3}\frac{k^2c_s^2a}{\Omega_m^0\mathcal{H}_0^2}. \quad (10)$$

Together, these equations provide a convenient way of obtaining the growth function

$$g(k, a) = \frac{Q(k, a)}{Q^0(k)} \exp\left(\int_1^a \frac{da'}{a'} \Omega_m(a')^{\gamma(k, a')}\right). \quad (11)$$

The explicit appearance of Q in this expression is due to our definition of g describing the growth of the total gravitational potential rather than of the matter perturbations only.

Of course, the growth function could easily be directly obtained by solving the linear perturbation equations numerically. For illustration, we show the linear matter power spectrum $P(k)$ for the

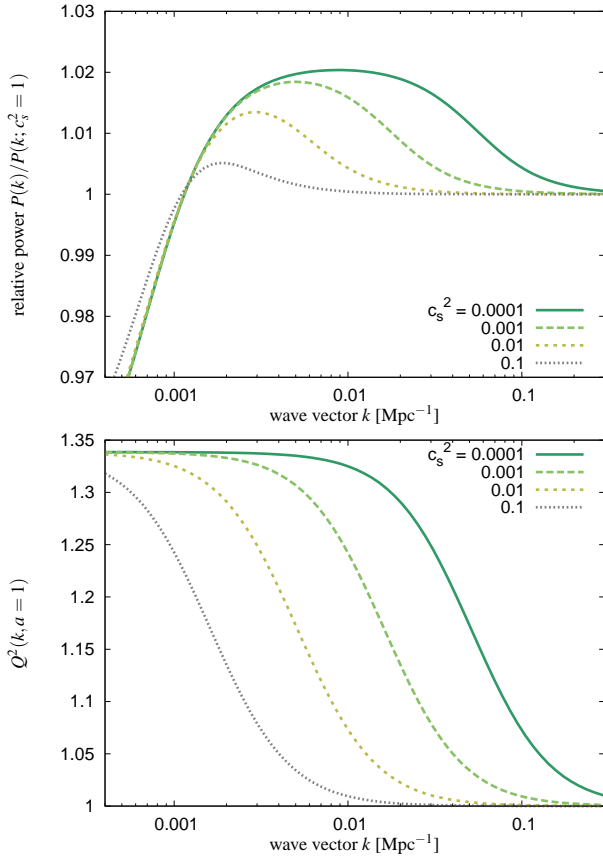


Figure 1. The upper figure shows the matter power spectrum $P(k)$ for $w = -0.8$ and varying dark energy speed of sound c_s^2 divided by the spectrum for $c_s^2 = 1$. The matter power spectrum is computed from the gauge-invariant density contrast $\Delta^{(m)}$. The lower figure shows the scale dependence of Q^2 for the same values of w and c_s^2 .

w CDM model for different sound speeds c_s^2 and $w = -0.8$ in Fig. 1. Here, we have used the code `CAMB` (Code for Anisotropies in the Microwave Background, Lewis et al. 2000), which has built-in facilities to work with the w CDM model with constant c_s^2 . We have assumed adiabatic initial conditions.

Perturbations in the dark energy act as an extra source of the gravitational potential in the Poisson equation (7) enhancing the growth of matter perturbations on subhorizon scales. This enhancement, however, is less than a percent effect for sound speeds $c_s^2 \gtrsim 0.1$ and restricted to large scales. The power spectrum $P(k)$ has to be known with very high precision in order to find significant constraints on c_s^2 . This becomes even more difficult for w closer to -1 , cf. Eq. (2). Note that the plot also shows superhorizon scales, where the results are gauge-dependent. For our analysis, we will use (subhorizon) scales k between 10^{-3} and 10^{-1} Mpc^{-1} .

With the parameterisation of $Q(k, a)$, Eq. (10), at hand, we can ask above which scale λ_{eff} dark energy clustering could leave observable traces. Let us make the heuristic assumption that the effect of a clustering dark energy component would be observable once roughly $Q(k, a = 1) \gtrsim 1 + \varepsilon$, with ε for example at the percent level. This is the case for scales

$$\lambda \equiv \frac{1}{k} \gtrsim \left(\frac{\varepsilon}{1 - \Omega_m^0} \right)^{1/2} \sqrt{\frac{2}{3}} \frac{1}{\sqrt{1+w}} \frac{|c_s|}{\mathcal{H}_0}. \quad (12)$$

For the exemplary values $\varepsilon \approx 1\%$ and $\Omega_m^0 \approx 0.3$, this defines a critical scale

$$\frac{\lambda_{\text{eff}}}{\mathcal{H}_0^{-1}} \approx 0.1 \frac{|c_s|}{\sqrt{1+w}} \quad (13)$$

with a similar behaviour as the scale given in Eq. (2). A precision experiment might be able to detect dark energy clustering if the effective scale λ_{eff} lies within the Hubble horizon. In particular, the common choice $w = -1$ refers to $\lambda_{\text{eff}} \rightarrow \infty$. This is already obvious from the parameterisation (10) yielding $Q = 1$ on all scales for $w = -1$. In this case, the sound speed becomes irrelevant and dark energy clustering cannot be detected.

3 3D WEAK COSMIC SHEAR

3.1 Convergence

In the presence of a gravitational lens, the observed image points θ of a galaxy differ from their true positions β . In a locally linear approximation, the mapping $\theta \mapsto \beta$ is described by a matrix

$$\mathcal{A} = \begin{pmatrix} 1 - \kappa - \gamma_1 & -\gamma_2 \\ -\gamma_2 & 1 - \kappa + \gamma_1 \end{pmatrix}. \quad (14)$$

The convergence κ determines the magnification of the image, the shear (γ_1, γ_2) determines its deformation. Both convergence and shear are calculated from second derivatives of the lensing potential ϕ , e. g.,

$$\kappa = \frac{1}{2} \Delta_{\theta, \varphi} \phi. \quad (15)$$

The lensing potential ϕ is a projection of the Newtonian gravitational potential Φ . In a flat universe,

$$\phi(\chi) = 2 \int_0^\chi d\chi' \frac{\chi - \chi'}{\chi \chi'} \Phi(\chi'), \quad (16)$$

where χ, χ' denote comoving coordinates. The convergence κ thus depends on the gravitational potential along the line of sight, which, in turn, is given by the density fluctuations. In this way, gravitational lensing can be used to probe the density field, without relying on galaxy bias models (Jain & Seljak 1997; Hu & White 2001). For general treatments of weak gravitational lensing, see Bartelmann & Schneider (2001); Bartelmann (2010b).

In a region of the sky covered by a weak lensing survey, the individual convergences κ and shears γ_i of the galaxies together allow to study the two-dimensional fields $\kappa(\vartheta, \varphi)$, $\gamma_i(\vartheta, \varphi)$. If the galaxies' distances are known (e. g. by a photometric redshift measurement), the fields become three-dimensional, $\kappa(\chi, \vartheta, \varphi)$, $\gamma_i(\chi, \vartheta, \varphi)$. 3d weak cosmic shear is a means to study the statistical properties of these fields (Heavens 2003; Castro et al. 2005).

The importance of the three-dimensional information for weak lensing precision tests of structure formation has first been studied for tomography (Hu 2002a). Also the use of spectroscopic redshifts instead of a photometric method has been considered (Ishak & Hirata 2005).

The statistics of the convergence field κ are hardly directly observable. But since the statistics of convergence and shear are equivalent, we may use the convergence κ instead of γ_i in our theoretical calculations.

The first step in a 3d weak cosmic shear calculation is a combined Fourier and spherical harmonic transform, $\chi \rightarrow k$, $(\vartheta, \varphi) \rightarrow (\ell, m)$,

$$\kappa_{\ell m}(k) = \sqrt{\frac{2}{\pi}} \int \chi^2 d\chi d\Omega \kappa(\chi, \vartheta, \varphi) j_\ell(k\chi) Y_{\ell m}^*(\vartheta, \varphi). \quad (17)$$

By means of the growth factor $g(k, a)$, we may replace the gravitational potential in Eq. (16) by the potential of today, $\Phi_{\ell m}(k) = g(k, a) \Phi_{\ell m}^0(k)/a$. Note that in clustering dark energy scenarios, the growth factor is scale-dependent. In the transformed variables, Eqs. (15), (16), and (7) take the simple forms

$$\kappa_{\ell m} = -\frac{\ell(\ell+1)}{2} \phi_{\ell m}, \quad (18)$$

$$\phi_{\ell m} = \eta_\ell(k, k') \Phi_{\ell m}^0(k'), \quad (19)$$

$$k^2 \Phi_{\ell m} = -4\pi G a^2 Q \rho_m \Delta_{\ell m}^{(m)}, \quad (20)$$

where we have, following Heavens (2003), introduced the quantity

$$\eta_\ell(k, k') = \frac{4}{\pi} \int_0^\infty \chi^2 d\chi j_\ell(k\chi) \int_0^\chi d\chi' \frac{\chi - \chi'}{\chi\chi'} j_\ell(k'\chi') \frac{g(k', a')}{a'} \quad (21)$$

and used the summation convention

$$A(k, k') B(k', k'') \equiv \int_0^\infty k^2 dk' A(k, k') B(k', k''). \quad (22)$$

The appearance of Q on the right-hand side of the Poisson equation accounts for the direct contribution, $\propto \rho_{DE} \Delta^{(DE)}$, of dark energy perturbations to the gravitational potential. The indirect and dynamical effect of dark energy clustering on the evolution of matter perturbations $\rho_m \Delta^{(m)}$ is accounted for by the modified growth index γ as outlined in Sec. 2.3.

3.2 Estimator

In Sec. 3.1, we have seen that the convergence $\kappa_{\ell m}(k)$ is intimately connected to the density fluctuation field $\delta_{\ell m}^0(k)$ by virtue of Eqs. (18) to (20). In other words, we can, e. g., use the convergence $\langle \kappa_{\ell m}(k) \kappa_{\ell' m'}(k') \rangle$ to probe the matter power spectrum $P^0(k)$.

Heavens (2003) has shown how to construct an appropriate estimator for a weak lensing survey including photometric redshifts. The two main ingredients of this estimator are:

(i) The inclusion of the uncertainty of the redshift measurement, for simplicity assumed to be a Gaussian with width σ_z equal for all galaxies,

$$p(\chi'|\chi) d\chi' = \frac{1}{\sqrt{2\pi}\sigma_z} \exp\left[-\frac{(z-z')^2}{2\sigma_z^2}\right] dz'. \quad (23)$$

We use a typical figure of $\sigma_z = 0.02$ (Heavens 2003). An extension of the formalism allowing for individual redshift errors is possible (Kitching et al. 2011).

(ii) The survey's galaxy distribution encoded in the number density $n(\chi) \equiv n(\chi)$ assumed rotationally symmetric. It constitutes a statistical weight favoring distances χ where the density of galaxies is higher. We use the forecasted shape

$$n(z) dz \propto z^2 \exp\left[-\left(\frac{z}{z_0}\right)^\beta\right] dz \quad (24)$$

for the Euclid survey. Here, we assume 100 galaxies per square arcminute, $z_0 = 0.64$, and $\beta = 3/2$, yielding a median redshift of $z_{\text{med}} = 0.9$ (Amara & Réfrégier 2007). For convenience, we consider the idealised case that the full sky is covered. For a realistic sky coverage $f_{\text{sky}} < 1$, the errors scale approximately by $f_{\text{sky}}^{-1/2}$.

We may then define the estimator $\hat{\kappa}_{\ell m}$ for the convergence $\kappa_{\ell m}$ in terms of the actual convergences κ_g of galaxies g as the harmonic transform

$$\hat{\kappa}_{\ell m}(k) = \sqrt{\frac{2}{\pi}} \sum_{\text{galaxies } g} \kappa_g j_\ell(k\chi_g) Y_{\ell m}^*(\vartheta_g, \varphi_g). \quad (25)$$

As explained above, the cosmic shear would be better suited for the analysis of actual observational data. The expectation value of $\hat{\kappa}_{\ell m}$ is

$$\bar{\kappa}_{\ell m}(k) = Z_\ell(k, k') M_\ell(k', k'') \kappa_{\ell m}(k''), \quad (26)$$

with the summation convention (22) and the quantities

$$Z_\ell(k, k') = \frac{2}{\pi} \int \chi'^2 d\chi' \int d\chi p(\chi'|\chi) j_\ell(k'\chi) j_\ell(k\chi), \quad (27)$$

$$M_\ell(k, k') = \frac{2}{\pi} \int \chi^2 d\chi j_\ell(k\chi) j_\ell(k'\chi) n(\chi), \quad (28)$$

taking account for the two main ingredients stated above. Abbreviating the product $B_\ell(k, k') \equiv Z_\ell(k, k'') M_\ell(k'', k''') \eta_\ell(k''', k')$, the covariance of $\hat{\kappa}_{\ell m}$ in terms of the matter power spectrum $P^0(k)$ reads

$$\begin{aligned} S_\ell(k, k') &\equiv \langle \hat{\kappa}_{\ell m}(k) \hat{\kappa}_{\ell m}(k') \rangle \\ &= A^2 B_\ell(k, k'') \frac{[Q^0(k'')]^2 P^0(k'')}{k''^4} B_\ell(k', k''') \end{aligned} \quad (29)$$

with $A = \frac{\ell(\ell+1)}{2} 4\pi G \rho_m^0$.

The full covariance $C_\ell(k, k')$ is obtained by adding the shot noise $N_\ell(k, k') = \frac{\sigma_e^2}{4} M_\ell(k, k')$ with $\sigma_e^2 = 0.1$ (Heavens 2003). This neglects the non-zero correlation between the ellipticities of neighbouring galaxies due to intrinsic alignments (Heavens et al. 2000; Schäfer 2009). This small-scale effect, however, does not affect our analysis of the large-scale consequences of a dark energy speed of sound. Further systematic effects have been studied (March et al. 2011) but, in general, do not seem to have a strong impact on parameter estimation (Huterer et al. 2006; Kitching et al. 2008; Takada & Jain 2009).

4 PARAMETER ESTIMATION

We apply a standard Fisher information matrix method to investigate possible future parameter constraints from upcoming weak lensing surveys. The Fisher information matrix $F_{\mu\nu}$ is a square matrix whose indices label (cosmological) parameters p_μ, p_ν . We choose the parameters $p_\mu, p_\nu \in \{\Omega_m, A_s, h, n_s, w, \log_{10} c_s^2\}$, assuming flatness: $\Omega_{DE} = 1 - \Omega_m$. The Fisher matrix determines stringent bounds on how precise a parameter p_μ can be constrained. If all parameters are estimated from the experimental data, the individual uncertainty Δp_μ does not go below the Cramér–Rao bound, $\Delta p_\mu \geq \sqrt{(F^{-1})_{\mu\mu}}$ (for an introduction, see Tegmark et al. 1997). The Cramér–Rao bound not only applies to individual parameters, but it also determines optimal confidence regions for a set of parameters. For two parameters p_μ and p_ν , the corresponding coefficients of F^{-1} are a quadratic form defining an error ellipse.

Formally, the Fisher matrix is defined via the likelihood L ,

$$F_{\mu\nu} = \left\langle -\partial_\mu \partial_\nu \ln L \right\rangle. \quad (30)$$

The likelihood $L \equiv L(\hat{\kappa}_{\ell m}|\mathbf{p})$ is the probability for an experiment to measure the value $\hat{\kappa}_{\ell m}$ for the estimator given cosmological parameters \mathbf{p} .

The cosmological parameters enter the likelihood in two ways. First, they predict a power spectrum $P^0(k)$ and a growth function $g(k, a)$, which, by Eq. (29), are decisive quantities for the covariance of the estimator. Second, they define the background evolution and hence the distance measures entering the quantities Z_ℓ , M_ℓ , and η_ℓ .

If the likelihood L is a multivariate Gaussian in the data with covariance matrix \mathbf{C} , the Fisher matrix is given by

$$F_{\mu\nu} = \frac{1}{2} \text{tr} \left[\mathbf{C}^{-1} (\partial_\mu \mathbf{C}) \mathbf{C}^{-1} (\partial_\nu \mathbf{C}) \right], \quad (31)$$

sensitive to the derivatives of the covariance \mathbf{C} with respect to the cosmological parameters.

For our estimator $\hat{\kappa}_{\ell m}(k)$, the covariance matrix carries the indices (ℓ, m, k, k') . Since different modes ℓ and m are uncorrelated, the covariance matrix \mathbf{C} splits into blocks. Further, the covariance $C_\ell(k, k')$ from Sec. 3.2 is assumed to be independent of m whereby all $2\ell + 1$ blocks for a given ℓ are identical. In terms of the covariance $C_\ell(k, k')$, we may reformulate Eq. (31) to

$$F_{\mu\nu} = \sum_{\ell=\ell_{\min}}^{\ell_{\max}} \frac{2\ell + 1}{2} \text{tr} \left(\mathbf{C}_\ell^{-1} \partial_\mu \mathbf{C}_\ell \mathbf{C}_\ell^{-1} \partial_\nu \mathbf{C}_\ell \right). \quad (32)$$

It should be kept in mind that the Cramér–Rao bounds are realistic estimates of the actual constraints only if the likelihood L as a function of the parameters \mathbf{p} is a Gaussian. This is often violated in the case of parameters that are difficult to measure and therefore weakly constrained, such as the sound speed parameter c_s^2 . The broad likelihood extends to regions where the dependence of the matter power spectrum $P(k)$ on c_s^2 , cf. Fig. 1, cannot be approximated linearly (Ballesteros & Lesgourgues 2010). This also affects the weak lensing convergence spectrum considered in this work. Figure 1 suggests that the logarithm $\log_{10} c_s^2$ is a more natural parameter to describe the reaction of the model to variations in the dark energy speed of sound. We thus choose $\log_{10} c_s^2$ as a model parameter in our analysis but emphasize that the Cramér–Rao bounds we calculate are only rough estimates of the actual future constraints.

A very practical feature of the Fisher matrix is its additivity. Given Fisher matrices $F_{\mu\nu}^{(A)}$, $F_{\mu\nu}^{(B)}$ for two independent experiments A and B , the joint Fisher matrix providing the combined parameter constraints is simply $F_{\mu\nu}^{(A+B)} = F_{\mu\nu}^{(A)} + F_{\mu\nu}^{(B)}$. This follows directly from the multiplication of the corresponding likelihoods and the definition of the Fisher matrix, Eq. (30). In our case, we can use this formalism to include prior information from other experiments than weak gravitational lensing.

As prior information, we use a Fisher matrix $F_{\mu\nu}^{(\text{CMB})}$ for the cosmic microwave background (CMB) based on forecasts for the Planck satellite. We include temperature (TT), polarisation (EE), and the cross-correlation spectrum (TE). We calculate the Fisher matrix $F^{(\text{CMB})}$ following Perotto et al. (2006). The predicted noisy spectra \tilde{C}_ℓ^{TT} (temperature only), \tilde{C}_ℓ^{EE} (E -mode polarisation), and \tilde{C}_ℓ^{TE} (cross-correlation) are encoded in a 3×3 matrix,

$$\mathbf{A}_\ell = \frac{2}{(2\ell + 1) f_{\text{sky}}} \times \begin{pmatrix} (\tilde{C}_\ell^{TT})^2 & (\tilde{C}_\ell^{TE})^2 & \tilde{C}_\ell^{TE} \tilde{C}_\ell^{TT} \\ (\tilde{C}_\ell^{TE})^2 & (\tilde{C}_\ell^{EE})^2 & \tilde{C}_\ell^{TE} \tilde{C}_\ell^{EE} \\ \tilde{C}_\ell^{TE} \tilde{C}_\ell^{TT} & \tilde{C}_\ell^{TE} \tilde{C}_\ell^{EE} & \frac{1}{2} \left[(\tilde{C}_\ell^{TE})^2 + \tilde{C}_\ell^{TT} \tilde{C}_\ell^{EE} \right] \end{pmatrix} \quad (33)$$

with a fraction f_{sky} of the CMB covered. From this, we evaluate the Fisher matrix,

$$F_{\mu\nu}^{(\text{CMB})} = \sum_{\ell=2}^{\ell_{\max}} \sum_{PP', QQ'} \partial_\mu \tilde{C}_\ell^{PP'} (\mathbf{A}_\ell^{-1})_{PP' QQ'} \partial_\nu \tilde{C}_\ell^{QQ'} \quad (34)$$

with the indices $PP', QQ' \in \{TT, EE, TE\}$.

Our forecast bases on expected properties of the Planck satellite (Hollenstein et al. 2009; Knox 1995). We adopt the expected in-

strument properties as listed in Table 1 of Hollenstein et al. (2009), namely a sky coverage $f_{\text{sky}} = 0.65$, a beam width $\theta_{\text{FWHM}} = 7$ arcmin, temperature noise $\Delta_T = 28 \mu\text{K arcmin}$, and polarisation noise $\Delta_E = 57 \mu\text{K arcmin}$. For the numerical calculation of the theoretically predicted multipoles, we employ CAMB.

5 METHOD

In principle, we have already collected the ingredients for our 3d weak lensing calculations, namely the covariance of the estimator, cf. Eq. (29), and the Fisher information matrix, Eq. (32). Due to the presence of multiple nested integrals, the actual calculation is involved and motivates the choice of adequate numerical approaches and techniques. We present our strategies in this section.

5.1 The quantities Z_ℓ , M_ℓ , and η_ℓ

The expectation value $\bar{\kappa}_{\ell m}$ of the 3d convergence estimator, Eq. (26), mainly is the application of Z_ℓ (27), M_ℓ (28), and η_ℓ (21) on today's gravitational potential $\Phi_{\ell m}^0(k)$,

$$\bar{\kappa}_{\ell m} \propto Z_\ell(k, k') M_\ell(k', k'') \eta_\ell(k'', k''') \Phi_{\ell m}^0(k'''), \quad (35)$$

where each multiplication corresponds to a k integration according to the convention, Eq. (22). We have introduced the shorthand $B_\ell(k, k''') \equiv Z_\ell(k, k') M_\ell(k', k'') \eta_\ell(k'', k''')$ for the product.

Before we explain an elaborate way to calculate B_ℓ with high precision, we first turn to a simplified approximate approach. Recalling that the sequence of functions

$$f_\ell(x) \equiv \sqrt{\frac{2}{\pi}} y \sqrt{\xi} j_\ell(\xi), \quad \xi \equiv y(x+1), \quad y \equiv \ell + \frac{1}{2} \quad (36)$$

approaches the Dirac delta function δ_D for $\ell \rightarrow \infty$, we may, for sufficiently large ℓ , use the approximation

$$j_\ell(k\chi) \approx \sqrt{\frac{\pi}{2}} \frac{1}{k \sqrt{y}} \delta_D \left(\chi - \frac{y}{k} \right). \quad (37)$$

In this approximation, the quantities Z_ℓ , M_ℓ , and η_ℓ take simple forms, namely

$$Z_\ell(k, k') \approx \frac{y}{k^3 k'} P \left(\frac{y}{k} \middle| \frac{y}{k'} \right), \quad (38)$$

$$M_\ell(k, k') \approx \frac{1}{k^2} n \left(\frac{y}{k} \right) \delta_D(k - k'), \quad (39)$$

$$\eta_\ell(k, k') \approx 2 \frac{k' - k}{k^3 k'} \frac{g(k', a(y/k'))}{a(y/k')} \text{ for } k \leq k', \text{ 0 else.} \quad (40)$$

Calculating the final product B_ℓ now does no longer pose difficulties,

$$B_\ell(k, k') \approx \frac{y}{k^3 k'} \frac{2g(k', a(y/k'))}{a(y/k')} \int_{\frac{y}{k'}}^{\infty} d\chi p \left(\frac{y}{k} \middle| \chi \right) n(\chi) \frac{\chi - \frac{y}{k'}}{\chi \frac{y}{k'}}. \quad (41)$$

We compare this approximate result with the full expression in Fig. 2.

Although useful for a first impression, these approximate results do not allow for a precision calculation of the covariance $C_\ell(k, k')$. We thus develop a more sophisticated strategy.

5.2 Covariance

The signal and noise parts of the covariance matrix are given in Sec. 3.2. While the noise part $\propto M_\ell$ is uncomplicated, the direct evaluation of the signal S_ℓ (29) would, in a first step, require

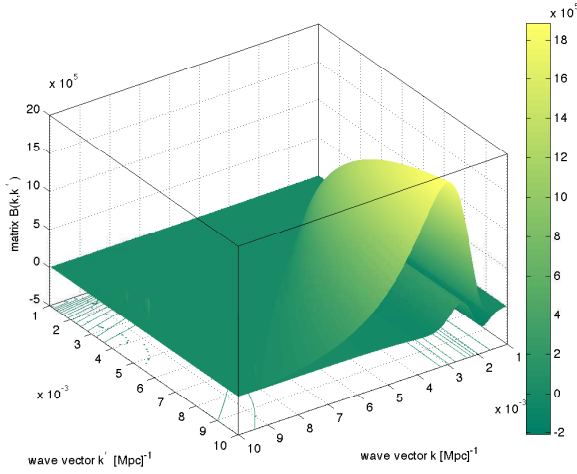


Figure 2. The matrix $B_\ell(k, k') = Z_\ell(k, k'') M_\ell(k'', k''') \eta_\ell(k''', k')$ for $\ell = 10$ (upper surface) with the difference between the full integration and the approximation given by Eq. (41) (lower surface and contours), which shows a small oscillatory feature close to the steep edge of $B_\ell(k, k')$ amounting to less than 10% of the amplitude.

the calculation of Z_ℓ , M_ℓ , and η_ℓ , which contain highly oscillating integrands, cf. Eqs. (27), (28), (21). In a second step, the product $B_\ell(k, k') \equiv Z_\ell(k, k'') M_\ell(k'', k''') \eta_\ell(k''', k')$ has to be calculated. Taken together, these are seven nested integrals. Calculating the signal covariance S_ℓ then requires two further integrations.

Fortunately, the orthogonality relation for spherical Bessel functions,

$$\int_0^\infty k^2 dk j_\ell(k\chi) j_\ell(k\chi') = \frac{\pi}{2\chi^2} \delta_D(\chi - \chi'), \quad (42)$$

can be used to solve several k integrals analytically. The remaining expression for B_ℓ reads

$$B_\ell(k, k') = \frac{4}{\pi} \int \chi'^2 d\chi' j_\ell(k\chi') \int d\chi p(\chi'|\chi) n(\chi) f_\ell(k', \chi), \quad (43)$$

where

$$f_\ell(k, \chi) \equiv \int_0^\chi d\chi' j_\ell(k\chi') \frac{\chi - \chi'}{\chi\chi'} \frac{g(k, a')}{a'}. \quad (44)$$

The number of nested integrals in the calculation of B_ℓ is reduced to three.

We will show that an efficient evaluation of the inner integral in Eq. (43) is possible using a Fast Fourier Transform (FFT). We therefore have to sample f_ℓ at discrete coordinates $\{\chi_j\}$. For each χ_j , we need not calculate the full integral (44) but only an integral from χ_{j-1} to χ_j . This is possible once we write the integral in a way that makes the integrand independent of the integral bound,

$$f_\ell(k, \chi) = \int_0^\chi \frac{d\chi'}{\chi'} j_\ell(k\chi') \frac{g(k, a')}{a'} - \frac{1}{\chi} \int_0^\chi d\chi' j_\ell(k\chi') \frac{g(k, a')}{a'}. \quad (45)$$

In redshift space, the conditional probability $p(z'|z)$ is a Gaussian, cf. Eq. (23). Inserting this property, we reformulate the inner integral in Eq. (43) as a convolution,

$$\int_0^\infty d\chi p(\chi'|\chi) n(\chi) f_\ell(k', \chi) = \int_0^\infty \frac{dz'}{d\chi'} \int_0^\infty dz p(z' - z) \times \left(\frac{d\chi}{dz} n(\chi(z)) f_\ell(k', z) \right). \quad (46)$$

For convolution integrals, fast solving methods exist. This is due to the convolution theorem stating that the Fourier coefficients of the individual functions can be multiplied to give the Fourier coefficients of the convolution. The Fourier transform of the Gaussian is again a Gaussian and thus analytically known. In the last factor, we use the sampled values of f_ℓ to perform a Fast Fourier Transform.

5.3 Fisher matrix

Once the covariance $C_\ell(k, k')$ is known, the Fisher matrix $F_{\mu\nu}$ can, in principle, be calculated according to Eq. (32). In terms of linear algebra, the Fisher matrix is given by a trace, which is a basis-independent operation. This opens the possibility of calculating the covariance in another basis, allowing for a more efficient numerical calculation.

Working with the tools of linear algebra, we find it more transparent to abandon the summation convention (22) for a moment and to work with standard notation instead. All earlier expressions can easily be reproduced if quantities of the type $A_\ell(k, k')$ are replaced by ordinary matrices

$$\mathbf{A}_{kk'}^\ell \equiv \sqrt{k^2 \Delta k} A_\ell(k, k') \sqrt{k'^2 \Delta k} \quad (47)$$

with a discrete step size Δk . The additional factors automatically reproduce the summation convention once a matrix multiplication is performed, $\sum_k k^2 \Delta k \rightarrow \int k^2 dk$.

Let us search for an orthogonal transformation \mathbf{T}^ℓ of the covariance matrix $\mathbf{C}_{kk'}^\ell = \sqrt{k^2 \Delta k} C_\ell(k, k') \sqrt{k'^2 \Delta k}$,

$$\tilde{\mathbf{C}}^\ell = (\mathbf{T}^\ell)^\dagger \mathbf{C}^\ell \mathbf{T}^\ell. \quad (48)$$

A good choice would, when applied on \mathbf{C}^ℓ , produce the orthogonality relation for spherical Bessel functions. Such a choice is given by

$$\mathbf{T}_{k\rho}^\ell = \sqrt{\frac{2}{\pi}} \sqrt{k^2 \Delta k} j_\ell(k\rho) \sqrt{\rho^2 \Delta \rho}. \quad (49)$$

The noise part $\mathbf{N}^\ell \propto \mathbf{M}^\ell$ becomes particularly simple,

$$\tilde{\mathbf{M}}_{\rho\rho'}^\ell = \sum_{k, k'} \mathbf{T}_{k\rho}^\ell \mathbf{M}_{kk'}^\ell \mathbf{T}_{k'\rho'}^\ell = n(\rho) \delta_{\rho\rho'}. \quad (50)$$

For the transformed signal part, $\tilde{\mathbf{S}}^\ell = (\mathbf{T}^\ell)^\dagger \mathbf{S}^\ell \mathbf{T}^\ell$, the product \mathbf{B}^ℓ is transformed from the left-hand side only,

$$\tilde{\mathbf{B}}_{\rho k'}^\ell = \sum_k \mathbf{T}_{k\rho}^\ell \mathbf{B}_{kk'}^\ell. \quad (51)$$

In fact, this transformation further simplifies \mathbf{B}^ℓ by virtue of the orthogonality relation,

$$\tilde{\mathbf{B}}_{\rho k'}^\ell = 2 \sqrt{\frac{2}{\pi}} \sqrt{\rho^2 \Delta \rho} \int_0^\infty d\chi p(\rho|\chi) n(\chi) \times \int_0^\chi d\chi' j_\ell(k'\chi') \frac{\chi - \chi'}{\chi\chi'} \frac{g(k', a')}{a'} \sqrt{k'^2 \Delta k}. \quad (52)$$

Applying the matrix $\mathbf{T}_{k\rho}^\ell$ introduced above on a quantity $\mathbf{A}_{kk'}^\ell$ can be understood as undoing the transformation $\chi \rightarrow k$ in the harmonic transform, cf. Eq. (17). This means that the Fourier mode k is replaced by a comoving distance, now labelled by ρ . Hence, the application of $\mathbf{T}_{k\rho}^\ell$ avoids unnecessary integrations originating from the harmonic transform.

Finally, we have all the necessary tools for an efficient calculation of the Fisher matrix at our disposal.

6 RESULTS

The Fisher matrix formalism, cf. Sec. 4, and our numerical methods, explained in Sec. 5, enable us to estimate which constraints on the dark energy sound speed will be possible with the weak lensing data of Euclid. The constraints depend, however, on the assumed fiducial parameters since the Fisher matrix is defined by derivatives at these points (31). Unfortunately, the dependence of sound speed constraints on the fiducial values of both the sound speed c_s^2 itself and the equation of state w is very strong. This is illustrated by the scale λ_{eff} introduced in Sec. 2.3, Eq. (13), below which dark energy clustering is not expected to be observable. This scale is a function of both c_s^2 and w , it exceeds the Hubble horizon for $c_s^2 \gg 1 + w$. In particular, the most natural fiducial value for w mimicking the standard Λ CDM model, i. e., $w \rightarrow -1$, is a singular choice, $\lambda_{\text{eff}} \rightarrow \infty$. The question of how well the sound speed c_s^2 can be constrained crucially depends on how close the equation of state w is to the value -1 .

In order to explore this behaviour quantitatively, we apply the Fisher matrix formalism to estimate the uncertainties of the dark energy sound speed and equation of state as functions of the fiducial values c_s^2 and w . In Sec. 4, we argued that a natural parameter to constrain is the order of magnitude $\log_{10} c_s^2$ rather than c_s^2 itself. The relative error on the sound speed approximately is $\Delta c_s^2 / c_s^2 \approx \ln(10) \Delta \log_{10} c_s^2$. This becomes imprecise for large uncertainties. In the case of the equation of state, we estimate $\Delta w / |w|$. For simplicity, we assume all other cosmological parameters to be exactly known, fixed to the WMAP7 recommended Λ CDM parameters (Komatsu et al. 2011).

The Fisher matrix is then a 2×2 matrix, and the uncertainties are estimated as explained in Sec. 4. We combine CMB and 3d weak lensing constraints. In our numerical calculation, the multipoles ℓ run from $\ell_{\text{min}} = 2$ to $\ell_{\text{max}} = 50$, the mode k from $k_{\text{min}} = 10^{-3} \text{ Mpc}^{-1}$ to $k_{\text{max}} = 10^{-1} \text{ Mpc}^{-1}$ in $N_k = 200$ equidistant steps. The included redshift range is $z_{\text{min}} = 10^{-4}$ to $z_{\text{max}} = 10$ in $N_z = 1000$ steps. For the CMB Fisher matrix, we include, as in all subsequent calculations, multipoles from $\ell = 2$ to $\ell = 2250$. The uncertainties are shown in Fig. 3. These results should be taken as a first approximation due to the limitations of the Fisher formalism when applied to weakly constrained parameters, cf. Sec. 4.

The lower figure, which shows the relative error $\Delta w / |w|$ on the dark energy equation of state w , is easily interpreted. The constraints on the equation of state parameter w are largely independent of the assumed sound speed c_s^2 . So, at least, the uncertainty in the sound speed c_s^2 does not worsen the accuracy with which w can be known, nor will a wrong assumption on c_s^2 introduce a significant bias on the estimate of w .

In the upper figure, we see that, conversely, the sound speed constraints heavily depend on the fiducial values, as explained above. For $w \gtrsim -0.95$ and sufficiently small c_s^2 the estimated error $\Delta \log_{10} c_s^2$ is smaller than one. We may thus hope that the combination of 3d weak cosmic shear and the CMB will determine the order of magnitude of c_s^2 .

For subsequent calculations, we choose the exemplary fiducial value $c_s^2 = 10^{-2}$. For w , the most natural choice, $w = -1$, is not adequate. If we still chose w close to -1 , e. g., $w = -0.99$ or $w = -0.9$, all results would strongly depend on the exact value chosen. Instead, we decide to go further away from the observationally preferred value and use $w = -0.8$ for illustration.

Adopting these choices for c_s^2 and w as the fiducial values, together with the Λ CDM WMAP7 recommended parameters (Komatsu et al. 2011), we now calculate the full Fisher matrices

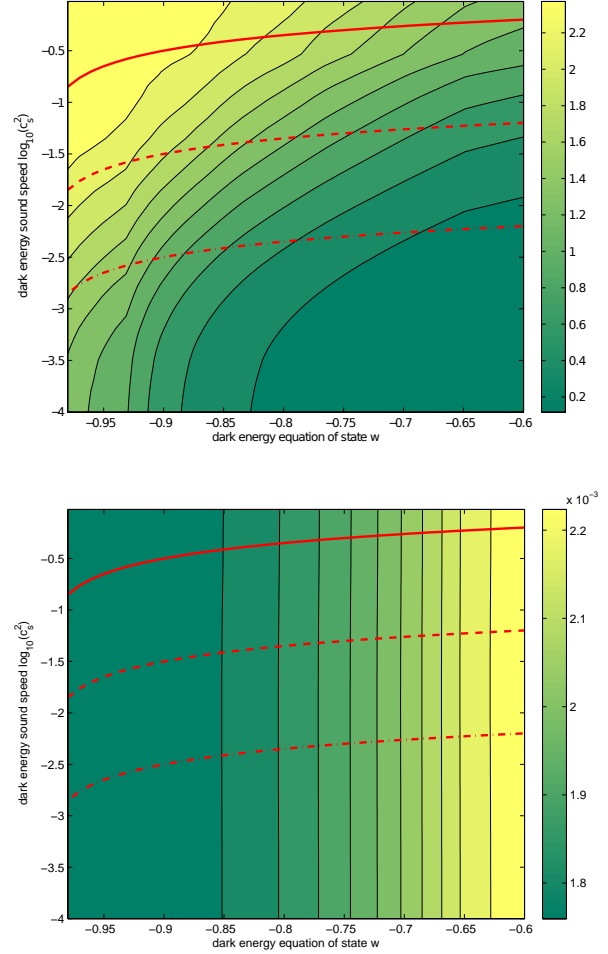


Figure 3. Cramér–Rao bounds on $\Delta \log_{10} c_s^2$ (upper figure) and $\Delta w / |w|$ (lower figure) for varying fiducial values w and $\log_{10} c_s^2$. The three red lines mark (from top to bottom) the scales $\lambda_{\text{eff}} = 10^{-n}$, $n = 1, 2, 3$ times the Hubble radius \mathcal{H}^{-1} according to Eq. (13) in the w - c_s plane.

for our six cosmological parameters: fractional matter density Ω_m , scalar initial perturbation amplitude A_s , Hubble parameter h , scalar spectral index n_s , equation of state w , and sound speed $\log_{10} c_s^2$. We choose higher numerical precision, $\ell_{\text{max}} = 300$ and $N_k = 500$, and avoid nonlinear scales. The resulting confidence regions for 3d weak cosmic shear alone and for the combined constraints with the CMB are seen in Fig. 4.

3d weak cosmic shear obviously provides interesting constraints on all the six cosmological parameters included in our analysis. Some constraints considerably improve when the CMB Fisher matrix is added. This is not true for the sound speed. We emphasize, of course, that our choice of fiducial parameters of w and c_s^2 is only illustrative. In more realistic cases $w \approx -1$, the constraints will be much weaker, cf. Fig. 3.

The Fisher matrix $F_{\mu\nu}$ for 3d weak lensing is obtained from a summation of all multipoles ℓ , cf. Eq. (32). It is instructive to examine which multipoles most contribute to the parameter constraints. We therefore plot the uncertainties of all the parameters as functions of the maximum multipole ℓ_{max} in Eq. (32), see Fig. 5.

Let us first consider the parameters other than c_s^2 . These show

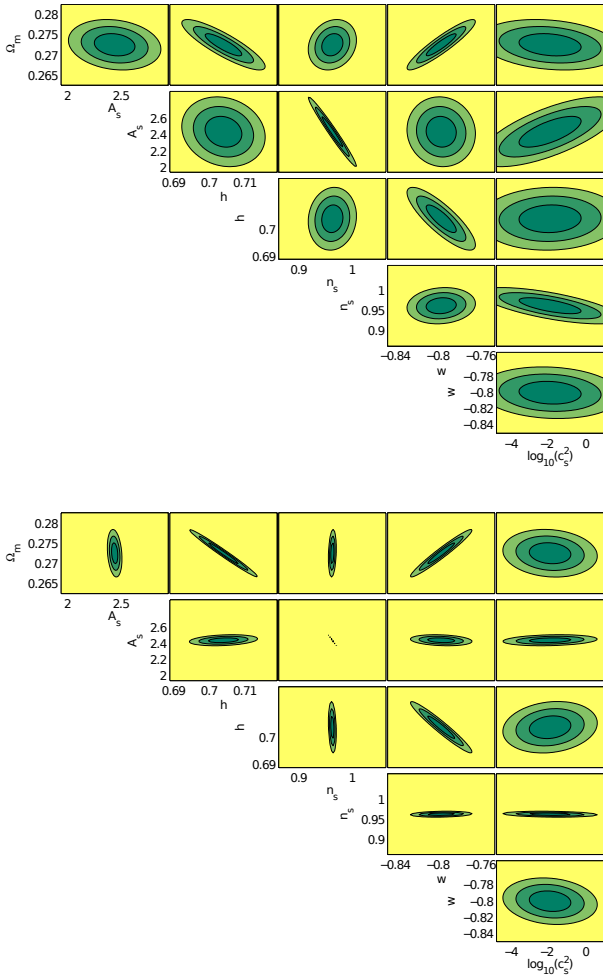


Figure 4. Estimated confidence ellipses (1σ , 2σ , and 3σ) for 3d weak lensing alone (upper figure) and combined with CMB prior (lower figure). The constraints on A_s have been rescaled by a factor of 10^9 .

two distinct behaviours. The constraints on the parameters w , Ω_m , and h are strongly improved by going to larger multipoles. The two parameters A_s and n_s characterising the primordial scalar perturbation spectrum are already tightly constrained for low multipoles. This is linked to the different sensitivities of the two independent observations, 3d weak lensing and the CMB, on these parameters. Looking again at the error ellipses in Fig. 4, we see that the constraints of 3d weak lensing alone on w , Ω_m , and h are not much weaker than the combined ones. Here, 3d weak lensing can establish strong constraints with increasing ℓ_{\max} . On the other hand, the CMB is more sensitive to A_s and n_s , whereby 3d weak lensing, regardless of ℓ_{\max} , cannot contribute very much to the constraints.

The case of the dark energy sound speed c_s^2 is different. The fact that the uncertainty does not decrease significantly with increasing $\ell_{\max} \gtrsim 20$ is mainly the consequence of clustering dark energy being a large-scale phenomenon, cf. Sec. 2.3 and Fig. 1. Plotting the covariances $C_\ell(k, k')$ of the estimator, see Sec. 3.2, for increasing multipoles ℓ , we see how the maximal sensitivity moves to smaller scales, Fig. 6. In fact, for low multipoles ℓ , 3d weak shear probes the scales of interest where dark energy clustering mainly occurs. The maxima seen in Fig. 6 are related to the fact that the

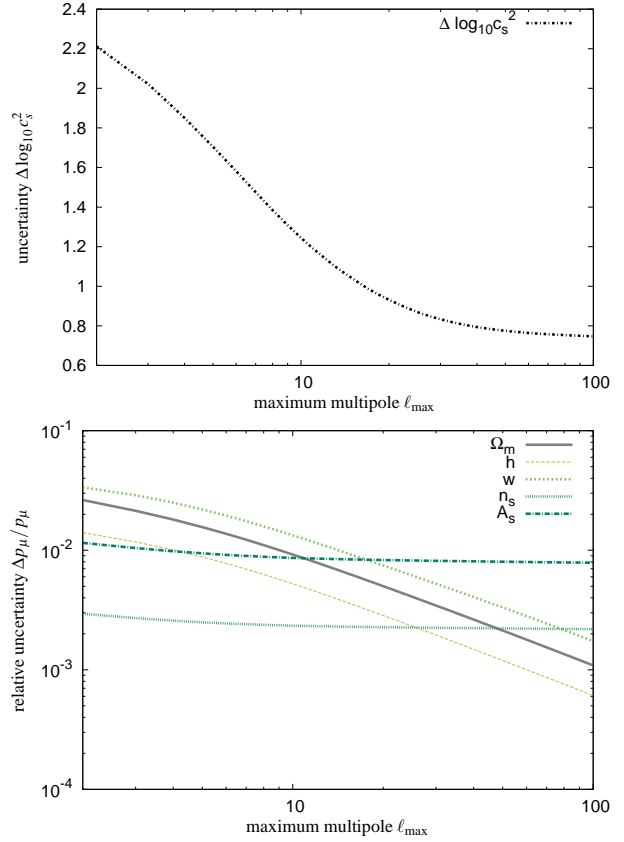


Figure 5. Marginalised uncertainties $\Delta \log_{10} c_s^2$ on the dark energy sound speed (top panel) and $\Delta p_\mu / p_\mu$ of the other cosmological parameters p_μ (bottom panel), depending on the maximum multipole ℓ_{\max} from 3d weak lensing with a CMB prior. Fiducial parameters: $w = -0.8$, $c_s^2 = 10^{-2}$. The CMB prior generally includes all multipoles from 2 to 2250.

galaxy distribution $n(\chi)$, Eq. (24), peaks at a comoving distance χ_* characterising the survey. Approximating Bessel functions by Dirac deltas, cf. Eq. (37), this distance roughly corresponds to the scale $k \approx \ell / \chi_*$. This explains the shift of the maximum for varying ℓ observed in Fig. 6.

Another way to study the ℓ dependence for the parameter constraints is to look at the direct contribution of a multipole ℓ to the diagonal elements $F_{\mu\mu}$ of the Fisher matrix, Eq. (32). These quantities can be interpreted as a (squared) sensitivity s_μ^ℓ per ℓ mode,

$$s_\mu^\ell \equiv \text{tr}(\mathbf{C}_\ell^{-1} \partial_\mu \mathbf{C}_\ell)^2 \quad (53)$$

Another way of interpreting Eq. (53) is that s_μ^ℓ describes the derivative of the measurement with respect to a cosmological parameter normalised by the noise of the measurement, such that it assumes large values for strong dependences of the signal on the cosmological model and small noise contributions. At the same time, s_μ^ℓ is the contribution to the Fisher matrix entry for the parameter p_μ from each mode $\kappa_{\ell m}$ of the convergence field. The number of modes for each ℓ is given by $2\ell + 1$.

We show the sensitivity s_μ^ℓ for the cosmological parameters in Fig. 7. Again, we observe that the sensitivity of 3d weak cosmic shear on the dark energy sound speed c_s^2 mostly comes from the first multipoles. This confirms the impression already obtained from the covariances $C_\ell(k, k')$ shown in Fig. 6, and emphasises the fact that the influence of a nontrivial sound speed is a large-scale

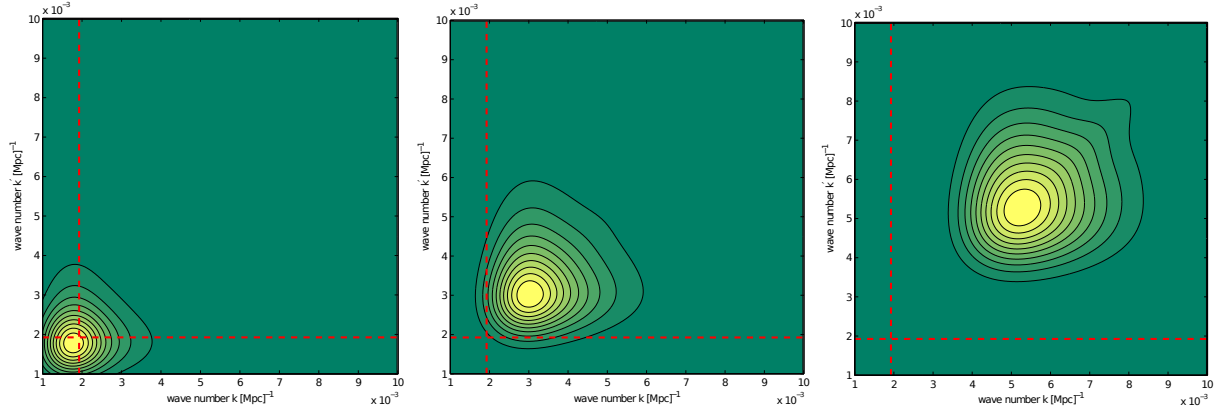


Figure 6. Qualitative results for the covariance $C_\ell(k, k')$ for $\ell = 5, 10, 20$ and $w = -0.8$. Brighter regions mark larger values. The red dashed lines mark the scales $k_{\text{eff}} = 1/\lambda_{\text{eff}}$ in the case $c_s^2 = 1$.

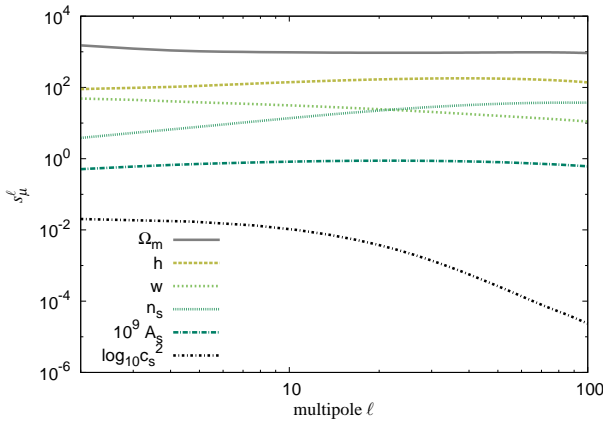


Figure 7. Sensitivity s_μ^ℓ as defined by Eq. (53) for the cosmological parameters. Fiducial values: $w = -0.8$, $c_s^2 = 10^{-2}$.

phenomenon. At the same time, the plot explains the two orders of magnitude difference in constraints on the dark energy sound speed compared to the other cosmological parameters.

7 SUMMARY

We have studied the potential of 3d weak cosmic shear to constrain a possible clustering of dark energy with the data of next generation surveys. We have parametrised the clustering dark energy component by two parameters characteristic for a generic cosmological fluid, its equation of state w and its (rest-frame) sound speed c_s^2 .

(i) For the 3d weak cosmic shear analysis, we have developed adequate numerical tools allowing for an efficient calculation of the covariance and Fisher matrices. These tools were shown to be numerically very efficient, which ultimately allowed us to sweep through the dark energy parameter space, while retaining sufficient numerical accuracy.

(ii) The capability of future observations to constrain c_s^2 , and thereby the clustering of dark energy, strongly depends on the dark energy equation of state w . If w is close to -1 , dark energy perturbations are mainly present at very large scales possibly outside the Hubble horizon. The effects of clustering dark energy would

hardly be observable at all if $c_s^2 \gg 1 + w$. As, indeed, current observations prefer values of w very close to -1 (Komatsu et al. 2011), this seems to be the decisive caveat.

(iii) Due to the sensitivity of sound speed constraints to the assumed exact value of w , we have estimated the uncertainties $\Delta \log_{10} c_s^2$ and $\Delta w/|w|$ as functions of the fiducial parameters (w, c_s^2), cf. Fig. 3. The numbers are combined constraints based on assumed properties of Euclid (Heavens 2003) and the Planck satellite (Perotto et al. 2006; Hollenstein et al. 2009; Knox 1995).

(iv) For the considered range of fiducial parameters ($-0.99 \lesssim w \lesssim -0.6$, $10^{-4} \lesssim c_s^2 \lesssim 1$), the estimated constraints on the sound speed $\Delta \log_{10} c_s^2$ vary between the extreme cases of 0.1 and 3. If $w \gtrsim -0.95$, the combination of Euclid and Planck is promising to constrain the order of magnitude of c_s^2 provided that the true sound speed is small enough. This would be considerable progress compared not only to constraints possible with current observational data (de Putter et al. 2010; Li & Xia 2010) but also, for most of the parameter space, to the constraints expected from weak lensing tomography and galaxy surveys alone (Sapone et al. 2010). Constraining c_s^2 within one or two orders of magnitude could also be possible with Planck and next-generation galaxy surveys (Takada 2006; Ballesteros & Lesgourgues 2010) or for neutral hydrogen surveys (Torres-Rodríguez & Cress 2007; Torres-Rodríguez et al. 2008). Although not our focus here, the constraints of 3d weak cosmic shear together with the Planck satellite on the dark energy equation of state w are worth mentioning; in fact, according to Fig. 3 and Fig. 4, w can be constrained below the percent level (for other constraints from 3d weak cosmic shear, see Heavens 2003; Heavens et al. 2006). Additionally, the true value of w largely determines the accuracy on the sound speed c_s .

There are two very different conclusions one could draw from these constraints on c_s^2 . First, we may regard $c_s^2 = 1$ and $w \approx -1$ as the natural values as they refer to unclustered dark energy such as a cosmological constant. Then, small deviations from $c_s^2 = 1$ are interesting; but these seem hardly observable in next generation experiments. Second, however, one may argue that c_s^2 is a completely unknown parameter with a natural range from 0 to 1; then, Euclid and 3d weak lensing could single out an order of magnitude in which c_s^2 lies. This could be a decisive step for discriminating between different dark energy models.

ACKNOWLEDGEMENTS

MW and YA acknowledge support from the DFG Transregional Collaborative Research Centre TRR 33, and BMS's work was supported by the German Research Foundation (DFG) within the framework of the excellence initiative through the Heidelberg Graduate School of Fundamental Physics. We would like to thank Matthias Bartelmann, Alessandra Grassi, and Angelos Kalivouris for their suggestions.

REFERENCES

- Amara A., Réfrégier A., 2007, MNRAS, 381, 1018 5
 Amendola L., 2000, Phys.Rev., D62, 043511 3
 Amendola L., Baldi M., Wetterich C., 2008, Phys.Rev., D78, 023015 3
 Amendola L., Kunz M., Sapone D., 2008, JCAP, 4, 13 1
 Ansari R. U. H., Unnikrishnan S., 2011, ArXiv e-prints 1104.4609 3
 Armendariz-Picon C., Mukhanov V. F., Steinhardt P. J., 2000, Phys.Rev.Lett., 85, 4438 3
 Armendariz-Picon C., Mukhanov V. F., Steinhardt P. J., 2001, Phys.Rev., D63, 103510 3
 Babichev E., Mukhanov V., Vikman A., 2008, JHEP, 0802, 101 3
 Ballesteros G., Lesgourgues J., 2010, JCAP, 1010, 014 6, 10
 Bartelmann M., 2010a, Reviews of Modern Physics, 82, 331 1
 Bartelmann M., 2010b, Classical and Quantum Gravity, 27, 233001 1, 4
 Bartelmann M., Schneider P., 2001, Physics Reports, 340, 291 4
 Bean R., Dore O., 2004, Phys.Rev., D69, 083503 1
 Bernstein G., Jain B., 2004, ApJ, 600, 17 1
 Caldera-Cabral G., Maartens R., Schäfer B. M., 2009, JCAP, 0907, 027 3
 Camera S., Kitching T. D., Heavens A. F., Bertacca D., Diaferio A., 2010, ArXiv e-prints 1002.4740 3
 Carroll S. M., 2001, Living Rev.Rel., 4, 1 1
 Castro P. G., Heavens A. F., Kitching T. D., 2005, Phys. Rev. D, 72, 023516 1, 4
 De Bernardis F., Martinelli M., Melchiorri A., Mena O., Cooray A., 2011, Phys. Rev., D84, 023504 3
 de Putter R., Huterer D., Linder E. V., 2010, Phys.Rev., D81, 103513 1, 10
 DeDeo S., Caldwell R., Steinhardt P. J., 2003, Phys.Rev., D67, 103509 1
 Erickson J. K., Caldwell R., Steinhardt P. J., Armendariz-Picon C., Mukhanov V. F., 2002, Phys.Rev.Lett., 88, 121301 1, 3
 Gordon C., Hu W., 2004, Phys.Rev., D70, 083003 2
 Hannestad S., Tu H., Wong Y. Y., 2006, JCAP, 6, 25 1
 Heavens A., 2003, MNRAS, 343, 1327 1, 4, 5, 10
 Heavens A., Refregier A., Heymans C., 2000, MNRAS, 319, 649 5
 Heavens A. F., Kitching T. D., Taylor A. N., 2006, MNRAS, 373, 105 1, 10
 Hollenstein L., Sapone D., Crittenden R., Schäfer B. M., 2009, JCAP, 4, 12 1, 6, 10
 Hu W., 1999, ApJL, 522, L21 2
 Hu W., 2002a, Phys. Rev. D, 66, 083515 2, 4
 Hu W., 2002b, Phys. Rev. D, 65, 023003 1
 Hu W., Scranton R., 2004, Phys.Rev., D70, 123002 1
 Hu W., White M., 2001, ApJ, 554, 67 4
 Huterer D., 2002, Phys. Rev. D, 65, 063001 1
 Huterer D., 2010, General Relativity and Gravitation, 42, 2177 1
 Huterer D., Takada M., Bernstein G., Jain B., 2006, MNRAS, 366, 101 5
 Huterer D., Turner M. S., 2001, Phys. Rev. D, 64, 123527 3
 Ishak M., Hirata C. M., 2005, Phys.Rev., D71, 023002 4
 Jain B., Seljak U., 1997, ApJ, 484, 560 4
 Jain B., Taylor A., 2003, Physical Review Letters, 91, 141302 1
 Kilbinger M., Benabed K., Guy J., Astier P., Tereno I., Fu L., Wraith D., Coupon J., Mellier Y., Balland C., Bouchet F. R., Hamana T., Hardin D., McCracken H. J., Pain R., Regnault N., Schultheis M., Yahagi H., 2009, A&A, 497, 677 1
 Kitching T. D., Heavens A. F., Miller L., 2011, MNRAS, 413, 2923 1, 2, 5
 Kitching T. D., Taylor A. N., Heavens A. F., 2008, MNRAS, 389, 173 5
 Knox L., 1995, Phys. Rev., D52, 4307 6, 10
 Kodama H., Sasaki M., 1984, Prog.Theor.Phys.Suppl., 78, 1 2
 Komatsu E., et al., 2011, ApJS, 192, 18 1, 2, 8, 10
 La Vacca G., Colombo L. P. L., 2008, JCAP, 0804, 007 3
 Lewis A., Challinor A., Lasenby A., 2000, ApJ, 538, 473 4
 Li H., Xia J.-Q., 2010, JCAP, 1004, 026 1, 10
 Linder E. V., Cahn R. N., 2007, Astropart.Phys., 28, 481 3
 March M. C., Trotta R., Amendola L., Huterer D., 2011, MNRAS, pp 612–+ 5
 Perotto L., Lesgourgues J., Hannestad S., Tu H., Wong Y. Y. Y., 2006, JCAP, 0610, 013 6, 10
 Ratra B., Peebles P., 1988, Phys.Rev., D37, 3406 2
 Sapone D., Kunz M., 2009, Phys. Rev. D, 80, 083519 3
 Sapone D., Kunz M., Amendola L., 2010, Phys. Rev. D, 82, 103535 3, 10
 Schäfer B. M., 2009, International Journal of Modern Physics D, 18, 173 5
 Schäfer B. M., Caldera-Cabral G. A., Maartens R., 2008, ArXiv e-prints 0803.2154 3
 Schäfer B. M., Heisenberg L., 2011, ArXiv e-prints 1107.2213 2
 Takada M., 2006, Phys.Rev., D74, 043505 10
 Takada M., Jain B., 2004, MNRAS, 348, 897 1
 Takada M., Jain B., 2009, MNRAS, 395, 2065 5
 Tegmark M., Taylor A. N., Heavens A. F., 1997, ApJ, 480, 22 5
 Torres-Rodriguez A., Cress C., 2007, MNRAS, 376, 1831 10
 Torres-Rodriguez A., Cress C., Moodley K., 2008, ArXiv e-prints 0804.2344 10
 Turner M. S., White M., 1997, Phys. Rev. D, 56, 4439 3
 Van Waerbeke L., Mellier Y., Erben T., Cuillandre J. C., Bernardeau F., Maoli R., Bertin E., McCracken H. J., Le Fèvre O., Fort B., Dantel-Fort M., Jain B., Schneider P., 2000, A&A, 358, 30 1
 Wetterich C., 1988, Nucl.Phys., B302, 668 2
 Wetterich C., 1995, A&A, 301, 321 3

This paper has been typeset from a $\text{\TeX}/\text{\LaTeX}$ file prepared by the author.